2260

Modelling of High-Power Continuous-Wave Tm:YAG Side-Pumped Double-Clad Waveguide Lasers

J.I.Mackenzie, C.Li and D.P.Shepherd

Optoelectronics Research Centre

University of Southampton

Southampton SO17 1BJ, UK

R.J.Beach and S.C.Mitchell

Maxios Laser Corporation

4749-A Bennett Drive

Livermore, CA 94550, USA

Abstract

A plane-wave model accounting for cross-relaxation, upconversion, ground-state depletion and gain saturation in cw laser systems is applied to side-pumped Tm:YAG double-clad planar waveguides. The temperature profile due to high-power pumping, and the delivery and absorption efficiencies of proximity-coupled diode bars are also calculated. The theoretical performance is found to be a good fit to the experimental results, which show 15W output at 2μm from 43W of diode pump power. The output channels for the absorbed power are quantified and it is shown that upconversion limits the gain and hence the size of the output coupling that can be used in such lasers. The same theory is then used to design a very compact waveguide laser capable of delivering 100W output power.

Index Terms – Lasers, waveguides, upconversion, laser thermal factors

1. INTRODUCTION

High power lasers at 2μm are of interest for several applications due to the strong absorption by water and human tissue, the low atmospheric absorption, and the eye-safe properties of light in this wavelength region. Operation of Tm:YAG on the $^3F_4 \rightarrow {}^3H_6$ transition is an attractive system for such lasers as it allows pumping by AlGaAs diodes around 0.8μm, while maintaining high efficiency and low thermal loading. This is possible, despite the large difference between the pump and laser photon energies, because of a favourable cross-relaxation process that leads to a pumping quantum efficiency approaching 2. The disadvantages of the Tm^{3+} system include its quasi-three-level nature, the presence of energy-transfer upconversion, and a relatively low emission cross-section.

End- and side-pumped bulk Tm:YAG lasers have been reported at continuous-wave (cw) powers of >100W using lens ducts [1] and parabolic concentrators [2] to achieve the required intense pumping density. Waveguide geometries have also been used for 2μm laser systems both in planar [3] and fibre [4] format. Recently, we have reported a double-clad Tm:YAG planar waveguide that delivers 15W output at 2μm when side-pumped by two 20W diode bars [5]. The double-clad waveguide has the advantage of allowing proximity-coupling of the diode-bars, leading to a very simple and compact device. Here, we model the performance of this laser, including the delivery and absorption of the pump power and the expected thermal load, in order to investigate its potential for power scaling. The laser model is a modified version of that presented by Beach [6], which accounts for ground-state depletion, gain saturation, cross-relaxation and upconversion. The model also allows easy identification of the channels into which the absorbed pump power is routed, clearly

demonstrating the regime in which upconversion can come to dominate the laser performance.

Following the introduction, this paper is organised as follows. Section II models the pump power delivery achieved though the proximity-coupling technique, giving the waveguide numerical aperture (*NA*) and coupling distance requirements for efficient pump launch. Beam propagation method (BPM) calculations are then used to model the absorption efficiency of the double-clad planar structure in comparison to that of uniformly doped material, demonstrating that taking the ratio of the doped to undoped areas is a very good approximation for the reduction in absorption coefficient. In section III, the cw theory of end-pumped quasi-three-level lasers presented by Beach [6] is modified to account for side-pumping, the double-clad waveguide geometry, and the presence of upconversion and cross-relaxation, to model the output power characteristics of the Tm:YAG waveguide laser. A very close fit is obtained using values for the propagation loss and upconversion coefficient in good agreement with those reported in the literature. We then identify the amount of power going into the output, upconversion, fluorescence, thermal and loss channels. Optimisation of the present system is also discussed. In section IV the thermal properties of the slab-like waveguide are discussed and fed back into the laser model of section III, allowing a design to be made for a compact 100W waveguide laser that is well within any limits imposed by the thermal loading. Finally, in section V we give our concluding remarks.

II. PUMP POWER DELIVERY AND ABSORPTION EFFICIENCY

A. Pump Power Delivery

The geometrical match between the emission aperture of a diode bar and the planar waveguides used in these experiments allows the use of proximity coupling, leading to very simple and highly compact laser systems. The waveguide design and the proximity coupling of a single diode bar to the double-clad structure are shown schematically in figure 1. In the experiments described here, the Tm:YAG double-clad waveguide was pumped from both sides by two diode bars from Coherent Inc. with a specified full-width half-maximum divergence, θ_{FWHM}, of 35° in the fast axis. Assuming a diffraction-limited Gaussian output beam from the diode in this axis, and an anti-reflection (AR) coated input face, we can make an estimate of the delivery efficiency into the central YAG layers using,

$$\eta_{del} = \frac{\int_{-\min\left(\vartheta_{inc},\sin^{-1}(NA)\right)}^{\min\left(\vartheta_{inc},\sin^{-1}(NA)\right)} \exp\left[-\ln(16)\left(\frac{\theta}{\theta_{FWHM}}\right)^2\right] d\theta}{\int_{-90}^{90} \exp\left[-\ln(16)\left(\frac{\theta}{\theta_{FWHM}}\right)^2\right] d\theta} \qquad (1)$$

where θ is the angle of propagation (in degrees) of the divergent diode beam with respect to the axis of the planar waveguide. If the half-angle subtended by the YAG central layers to the diode emission aperture, θ_{inc}, is smaller than the angular acceptance of the waveguide, $sin^{-1}NA$, then (1) describes the overlap of the diverging pump beam with the physical aperture of the YAG central layers. Any light incident on the waveguide outside this aperture is lost. If the angular acceptance of the waveguide is less than θ_{inc} then (1) describes the fraction of the diverging pump beam that is contained by the numerical aperture of the YAG/sapphire waveguide. In our experimental set up (θ_{inc}=56°, NA=0.47) it is the latter condition that applies. Eqn.(1) will slightly underestimate the delivery efficiency due to the fact that pump light propagating at angles larger than the waveguide NA is not totally lost, as partial

reflection will still occur at each bounce from the YAG/sapphire interface. A very small contribution would also be made to the absorbed power by light reflecting from the upper sapphire/air interface. Figure 2 shows how the delivery efficiency varies with diode coupling distance, D, and the waveguide NA. It can be seen that the delivery efficiency saturates as the NA is increased for a given coupling distance, and as the coupling distance is reduced for a given NA. It also shows, that for the particular values of diode beam divergence and waveguide dimensions used here, the coupling efficiency approaches 100% when the coupling distance is <20μm and the numerical apertures is >0.6. A delivery efficiency of 0.942 is calculated for our combination of coupling distance (10μm) and NA (0.47).

Figure 3 shows the results of BPM modelling, using a commercial software package from Kymata Software, of the calculated pump intensity at the end of the waveguide (assuming no absorption and infinitely thick sapphire layers), which shows how the remaining ~5% of the pump light is lost to radiation modes. The real value of the delivery efficiency may vary from this figure due to non-diffraction-limited beam quality from the diode, reflections from the AR coating, and (as previously discussed) reflection of power beyond the NA of the waveguide. Nevertheless, it is clear that this is a very compact and efficient method of pump delivery.

B. Absorption Efficiency

A simple assumption can be made that the absorption coefficient of the pump radiation delivered to the waveguide will be reduced by a factor, η_{po}, equal to the ratio of the doped to undoped area of the YAG layers, compared to uniformly doped material. However, this assumption does not account for the different overlap of the various propagation modes allowed by the waveguide with the central doped region. With this in mind we used BPM to

compare the absorption efficiency of the structure shown in figure 1 to a similar structure with uniform doping throughout the YAG layers. The results, shown in figure 4, show that the absorption coefficient is reduced by η_{po}=0.68 whereas the simple assumption above leads to a value of 0.67. The very small difference in these figures is due to the larger absorption coefficients of lower order modes, which approach that of uniformly doped material, compared to those of higher order modes. This modelling is based on a perfectly aligned diode, which leads solely to the excitation of even modes within the YAG layers. However, the same modelling for a diode offset vertically by 5μm, so that the odd modes are also excited, gives nearly identical results.

III. LASER PERFORMANCE

A. Output Power

The laser performance of the 1cm long double-clad Tm:YAG waveguide shown in figure 1, when pumped from both sides with two 20W diode bars, was compared to predictions based on a quasi-three level laser model [6]. This plane wave model, modified to account for cross-relaxation and upconversion in the Tm^{3+} system and the side-pumped geometry, is likely to be a good approximation due to the relatively uniform nature of the gain distribution and laser saturation. In the guided plane this is due to the double-clad waveguide structure. For the 10at%-doped, 5mm-wide, double-clad waveguide and the R=0.9 output coupler used in our experiments, the single-pass pump absorption (see appendix) is calculated to be 0.73 (compared to a non-saturated absorption of 0.756), in good agreement with experimental observation. Thus, the double-sided pumping will also give a relatively uniform gain profile in the non-guided plane (we calculate a 24% variation in the upper-laser-level population density across the width of the guide for the case of unsaturated pump absorption).

The laser saturation of the gain in the non-guided direction will also be relatively plane wave in nature, due to the highly multi-mode output in this axis. The model also allows easy identification of the various channels into which the absorbed pump power is routed. The details of the modified model are given in the appendix while here we present the main results and the parameters used.

The Tm:YAG energy levels and the pumping, cross-relaxation, upconversion and lasing processes are shown in figure 5. The output power of the laser is related to the incident pump power, P_p, by

$$P_{out} = \eta_{slope}(P_p - P_{th}) \tag{2}$$

where the slope efficiency, η_{slope}, with respect to incident power is

$$\eta_{slope} = \eta_{QY}\eta_{\mathrm{mod}\,e}\eta_{del}\frac{\nu_l}{\nu_p}\left(\frac{1-R}{R}\right)\left(\frac{1-e^{\sigma_p N_{2p}\eta_{po}}}{\left(e^{\sigma_l N_{2l}\eta_{lo}}-1\right)\left(1+T^2 e^{\sigma_l N_{2l}\eta_{lo}}\right)}\right), \tag{3}$$

and the threshold incident power, P_{th}, is

$$P_{th} = \frac{h\nu_p}{\eta_{QY}\eta_{del}\tau_{eff}}\left(\frac{n_2 LWd_{core}}{1-e^{\sigma_p N_{2p}\eta_{po}}}\right). \tag{4}$$

In (3) and (4), n_2 is the population density of the excited state manifold given by

$$n_2 = \frac{1}{f_a^l + f_b^l}\left(\frac{1}{2\eta_{lo}\sigma_l L}\ln\left(\frac{1}{T^2 R}\right) + f_a^l n_o\right) \tag{5}$$

and N_{2p} and N_{2l} are the integrated inversion densities (with respect to width, W, and length, L, respectively), and are referenced to the Stark levels coupled by the pump and laser radiation as below,

$$N_{2p} = f_a^p (n_2 - n_o) W \tag{6}$$

$$N_{2l} = (f_a^l + f_b^l) n_2 L - f_a^l L \tag{7}$$

Here, n_o is the lasing dopant density, f_a^l is the terminal laser Stark level Boltzmann occupation factor, f_b^l is the initial laser Stark level Boltzmann occupation factor, and f_a^p is the initial pump Stark level Boltzmann occupation factor.

Table 1 gives a list of the parameters used in (3) - (7). The quantum yield, which accounts for the cross relaxation process shown in figure 5, is set at 1.98 using the data presented by Honea et al [1] and accounting for our doping level of 10 at.%. The mode fill efficiency is set at 1 as the laser mode is expected to efficiently sweep out the available gain due to the double clad structure and its multi-mode nature in the non-guided axis. The emission and absorption cross-sections are set relative to the Boltzmann occupation factors [1],[6]. The overlap of the pump with the doped area was discussed in section II and the overlap of the laser with the doped area is calculated assuming that the laser operates on the fundamental guided mode (as found experimentally). The Boltzmann factors are calculated using the Stark splittings reported by Gruber et al [7], and assuming an average operating temperature of 306K (see section III).

The values for the effective lifetime and waveguide transmission are found by fitting to the experimental laser performance as shown in figure 6. The effective lifetime of 2.1ms is

related to the low-excitation $^3F_4$ lifetime, τ_2=10.5ms, and the upconversion rate coefficient, k, by

$$\tau_{eff} = \frac{1}{\frac{1}{\tau_2} + kn_2}. \tag{8}$$

Here, k represents an overall value accounting for both the upconversion processes shown in figure 5. Rustad and Stenersen [8] have shown that the overall upconversion is dominated by k_{23} and values for this coefficient against doping level are given by Shaw et al [9]. The fit to experimental results leads to a value for k of $3.6\text{x}10^{-24}$ m^3s^{-1}, which is in good agreement with the published data for a doping level of 10at.%. The fitted one-way transmission corresponds to a propagation loss coefficient at 2.02μm of 0.04dB/cm. This is somewhat lower than the values found at 1μm for similar Nd and Yb-doped double-clad waveguides [10],[11] (0.2dB/cm) and is approaching reported values at 1μm for bulk Nd:YAG rods [12] (0.03dB/cm). The excellent fit to the experimental results using very reasonable parameter values allows predictions to be made for optimisation and power scaling of this system with some confidence.

B. Output Channels for Input Power

The model allows for easy identification of the routing of the input pump power into the various possible output channels. Here, the output channels are identified as the output power, given by (2), the fluorescence power,

$$P_{fl} = \frac{h\nu_1 n_2}{\tau_2} LWd_{core} \tag{9}$$

the upconversion power,

$$P_{up} = h\nu_l n_2^{\,2} kLWd_{core} \tag{10}$$

the quantum-defect thermal power,

$$P_{therm} = \eta_{del} P_p \left(1 - e^{\eta_{op}\sigma_p N_{2p}}\right)\left(1 - \frac{\eta_{QY}\nu_l}{\nu_p}\right) \tag{11}$$

and the power loss,

$$P_{loss} = P_p \left(\frac{R}{1-R}\right)\left(1 - T^2\right) e^{\eta_{ol}\sigma_l N_{2l}} . \tag{12}$$

Figure 7 shows a plot of these various output channel powers against output coupling for the maximum experimental input power of 43.8W. The graph shows that the use of a R=0.9 output coupler is near optimum for this pump power level and that the power going to heat at this point is nearly 7W. It should be noted that a certain fraction of the upconversion power will also be converted to heat due to non-radiative decay of the ions promoted into the $^3H_5$ level. However, at optimum output coupling this contribution to the total heating power is small compared to the quantum-defect thermal power given in (11), and has been neglected in our thermal calculations (section IV). It can also be seen that the range of output coupling, and hence the achievable gain, is limited due to upconversion becoming the dominant output channel for the absorbed pump power. This is confirmed by figure 8 where the theoretical

output power is plotted against output coupling for various values of the upconversion rate coefficient. Our experimental observation that we were unable to obtain lasing with a 50% output coupler is therefore attributed to the presence of upconversion. Similar effects due to energy-transfer upconversion have also recently been described in cw Nd^{3+}-doped lasers [13]. The main reason for the drop in output power at low reflectivity for the case where no upconversion is present is depletion of the ground state leading to a smaller absorption efficiency.

C. Optimisation of doping level

At this point it is interesting to consider what is the optimum Tm doping level. If it is increased from the current 10at.% doping level we should decrease the width of the guide in order to maintain the same fractional power absorption and hence the relatively uniform gain distribution. Reducing the width would also help to decrease the Fresnel number of the cavity and hence improve the M^2 of the output in the non-guided plane. However, this would bring with it a penalty in terms of increased upconversion coefficients [9] and a greater thermal load per unit volume. Consequently, a drop in output power of nearly 1W is expected by going to a 15at.% doping level. If we reduce the doping level from 10at.% we are forced to increase the width of the guide to maintain the same pump absorption efficiency, which in turn would adversely effect the output M^2 value. An initially very slight reduction in the quantum yield would also occur[1] but we would nevertheless expect an increase in output power, due to reduced upconversion and thermal load, of ~0.5W by going to a 5at.% doping level.

IV. THERMAL PROPERTIES AND POWER SCALING

Planar waveguide lasers have been shown to exhibit similarly good thermal management properties to bulk slab lasers [14], [15]. Here, we model the temperature rise in our particular structure and its implications for power scaling to the 100W level. A simple 1-D model [14], [15] based on the architecture shown in figure 9 and using the parameters listed in table 2 gives the temperature distribution near the core shown in figure 10.

The value of Q used in this model is based on a thermal power of 3.4W. This is chosen to calculate the temperature used in the laser model (306K) as an average figure between zero and full pumping power when 6.8W of thermal power is predicted. The temperature in the core is predicted to be ~324K (51°C) at full pump power. It should be made clear that the cooling arrangement and the waveguide structure is not optimised in terms of minimising the temperature rise. For instance, with both faces heat sunk and the use of 100μm-thick substrate and cladding layers (which would still give a robust and easy to handle device looking somewhat like a microscope cover slip) the temperature at maximum pump power is only 28°C, for a heat sink temperature of 16°C.

At this point it is useful to enquire into the power scaling of such a device. A simple analysis [15] suggests that, with the current thermal load and the thin, double-face-cooled waveguide described above, we would be three orders of magnitude below the surface stress fracture limit. Similarly, thermal lensing will be dominated by the guidance at such thermal power densities [15]. For the bonded waveguides described here, the different thermal expansion coefficients of the YAG and sapphire layers is a potential limitation but, in practice, they can clearly survive high temperatures as part of the fabrication process involves annealing the structure at a few hundred degrees. Thus, the main thermal limitation for quasi-three-level lasers will be degradation in the laser performance due to increased population in

the lower laser levels. As an example, figure 11 shows the expected laser performance for a range of temperatures (not accounting for any change in emission cross-section with temperature).

The simplest scaling from our present results could be obtained by replacing the two 20W diodes with two 60W diodes, which are readily available with similar emission apertures. For the thin, double-face-cooled, waveguide this would give a maximum temperature of 321K and an expected output power of 50W for an output coupler of R=0.87. Scaling from this point, without increasing the thermal load per unit volume, and hence the temperature rise, could be achieved through increasing the length of the crystal and adding more diode pumps. Figure 12 gives the expected laser performance for a 2cm long device, side-pumped by four 60W diodes, showing a maximum of 100W output power for a R=0.75 output coupler. The output characteristic of this waveguide has important implications for which method could be used to control the spatial properties of the laser in the non-guided plane. Typically, the combination of side-pumping with the plane/plane laser resonator used here leads to highly multi-mode output in the non guided plane [5], [10], [15]. It has been proposed [16] that monolithic hybrid guided/unstable resonators would be a potential solution to this problem because of the high gains available from diode-pumped waveguide lasers. However, in the case of Tm:YAG, the fact that optimum output powers occur for relatively low output coupling, due to upconversion, means that the potential for use of unstable resonators will be limited. However, the very low propagation loss found here suggests that zig-zag-path stable cavities should be feasible for control of the non-guided spatial mode.

V. CONCLUSIONS

We have successfully applied a plane-wave model for cw operation of quasi-three-level lasers to a side-pumped double-clad Tm:YAG waveguide laser. The model accounts for the ground-state depletion, gain saturation, cross-relaxation and upconversion. We have also accounted for the pump delivery efficiency, which is found to be >90%, the effect of the double-clad structure on the pump absorption, for which simply taking the ratio of doped to undoped areas is shown to be a good approximation, and the thermal loading associated with high-power operation. A very good fit is obtained to the experimentally observed result of 15W output power at 2.02μm for 44W of diode pump power at 785nm. The fit arrives at values of 0.04dB/cm for the propagation loss at 2μm and an upconversion rate coefficient of 3.6×10^{-24} $m^3 s^{-1}$, which is in good agreement with previously reported values. The modelling also shows that the optimum output coupler reflectivity for the 10at.%-doped Tm:YAG laser remains at relatively high values, even for >200W pump power, due to the effect of upconversion. If a lower dopant concentration were used to lessen the effect of upconversion, the effects of ground-state depletion would be the limiting factor. The prospects for power scaling of the planar waveguide laser are shown to be very good with the expectation that structures with dimensions (including the sapphire substrate and overlay layers) of a ~200μm by 5mm by 2cm could be efficiently side-pumped by four 60W diode bars to give 100W output power at 2μm with temperature rises in the core of ~30°C.

It is important to note that at this point, although the output is diffraction-limited in the guided plane due to the double-clad structure, the laser output remains highly multi-mode in the non-guided plane. From the laser modelling it is suggested that the potential for the use of unstable resonators to solve this problem is limited due to the effects of upconversion on the

available gain. However, the very low propagation loss found in these waveguides indicate that it is possible to use a longer zig-zag lasing path to efficiently sweep out the broad gain area, which in turn would allow the use of a stable resonator. The fabrication of monolithic resonators to maintain the advantages of the highly compact design, along with the proposed power scaling, is currently under investigation.

APPENDIX

Eqns. (2)-(4) are derived for steady-state laser operation by setting the rate of excitation of the laser ions, R_{ex}, equal to the rate of de-excitation, $R_{de\text{-}ex}$, and by assuming that the entire lasant population (density n_0) is contained within the $^3H_6$ (density n_1) and $^3F_4$ (density n_2) manifolds.

A. Rate of excitation

The fraction of incident pump power delivered to the waveguide (see section II) that is absorbed in a single pass across the width of the waveguide is

$$F_A = 1 - e^{\left(-\sigma_p \eta_{po} \int_0^W f_a^p n_1 dy\right)} \tag{A1}$$

where the y-axis corresponds to integration across the width of the guide. As we know all the population lies within the first two manifolds we can write,

$$-f_a^p n_1 = f_a^p (n_2 - n_o) \tag{A2}$$

and using the definition given in (6) we have,

$$F_A = 1 - e^{\sigma_p N_{2p} \eta_{po}}. \tag{A3}$$

The rate at which the lasant ions are promoted into the upper laser level is then given by,

$$R_{ex} = \eta_{QY}\eta_{del}\frac{P_p}{h\nu_p}\left(1 - e^{\sigma_p N_2 p \eta_{po}}\right). \tag{A4}$$

B. Rate of De-excitation

The fraction of laser power absorbed in a single pass along the length of the waveguide is,

$$F_B = 1 - e^{\left(-\sigma_l \eta_{lo}\int_0^L \left(f_a^l n_1 - f_b^l n_2\right)dx\right)} \tag{A5}$$

where the x-axis corresponds to integration along the length of the guide. We then note that,

$$f_b^l n_2 - f_a^l n_1 = (f_a^l + f_b^l)n_2 - f_a^l n_o \tag{A6}$$

which, in combination with the definition given in (7), gives,

$$F_B = 1 - e^{\sigma_l N_2 l \eta_{lo}}. \tag{A7}$$

By tracing the laser power reflected back from the output coupler through the cavity, and assuming that the propagation losses can be lumped into a one-way cavity transmission located at the high reflector, the de-excitation rate is given by,

$$R_{de-ex} = \frac{P_{out}}{\eta_{mode} h\nu_l}\left(\frac{R}{1-R}\right)\left(e^{\sigma_l N_2 l \eta_{lo}} - 1\right)\left(1 + T^2 e^{\sigma_l N_2 l \eta_{lo}}\right) + \frac{n_2 LWd_{core}}{\tau_{eff}}. \tag{A8}$$

Equating (A8) and (A4) then gives eqns.(2)-(4) for the laser output power, threshold and slope efficiency.

C. Excited-State Population Density

In order to calculate (2)-(4) we must also use (5) to find the excited-state population density. In the steady-state this is given by,

$$T^2 \mathrm{Re}^{2\sigma_l N_{2l} \eta_l} = 1. \qquad \text{(A9)}$$

Re-arranging (A9) and expressing N_{2l} as given in (7) then leads to the expression given in (5).

ACKNOWLEDGEMENT

This work was funded in part by a UK EPSRC grant, number GR/M98449/01. The portion of this work carried out at Maxios was supported by Eglin Air Force Base under contract #F08630-99-C-0016.

Table Captions

Table 1 Laser Model Parameters

Table 2 Thermal Model Parameters

Table 1

Quantum yield	η_{QY}	1.98
Mode fill efficiency	η_{mode}	1
Delivery efficiency	η_{del}	0.94
Pump 785nm photon energy	$h\nu_p$	$2.5\text{x}10^{-19}$ J
Laser 2.02μm photon energy	$h\nu_l$	$9.8\text{x}10^{-20}$ J
Output Coupler Reflectivity	R	0.9
Pump absorption cross-section	σ_p	$1.01\text{x}10^{-24}$ m^2
Pump overlap with doped region	η_{po}	0.68
Laser emission cross-section	σ_l	$2.7\text{x}10^{-25}$ m^2
Laser overlap with doped region	η_{lo}	0.96
One-way waveguide transmission	T	0.99
Effective excited state storage lifetime	τ_{eff}	$2.1\text{x}10^{-3}$ s
Waveguide length	L	$1\text{x}10^{-2}$ m
Waveguide width	W	$5\text{x}10^{-3}$ m
Doped core diameter	d_{core}	$20\text{x}10^{-6}$ m
Tm doping density	n_o	$1.38\text{x}10^{27}$ m^{-3}
Terminal laser Stark level Boltzmann occupation factor at 306K	f_a^l	0.019
Initial laser Stark level Boltzmann occupation factor at 306K	f_b^l	0.451
Initial pump Stark level Boltzmann occupation factor at 306K	f_a^p	0.296

Table 2

Air temperature	T_a	293 K
Heat sink temperature	T_{hs}	289 K
Air heat transfer coefficient	λ_a	10 $Wm^{-2}K^{-1}$
Water-cooled heat sink heat transfer coefficient	λ_{hs}	6000 $Wm^{-2}K^{-1}$
Thermal conductivity of YAG	k_y	13 $Wm^{-1}K^{-1}$
Thermal conductivity of sapphire	k_s	35 $Wm^{-1}K^{-1}$
Thermal power loading per unit volume	Q	$3.4x10^9$ Wm^{-3}

Figure Captions

Figure 1 Schematic diagram of proximity-coupling a diode bar to a double-clad Tm:YAG waveguide.

Figure 2 Delivery efficiency against coupling distance and waveguide numerical aperture.

Figure 3 Calculated pump power distribution at the end of the waveguide assuming no absorption (NB logarithmic scale).

Figure 4 Absorption of pump radiation against distance in units of absorption length (l_{abs}). Dashed lines are the calculated power and the solid lines are linear fits. The upper two curves show the absorption in uniformly doped and centrally doped waveguides. The lower two curves show the absorption of the lowest order mode and a higher order mode in the centrally doped waveguide.

Figure 5 Schematic diagram of the Tm:YAG energy levels involved in the 2μm laser operation. The upconversion and cross-relaxation processes considered in the model are indicated on the left and the Boltzmann occupation factors of the relevant Stark levels at 306K are shown on the right.

Figure 6 Output power against pump power.

Figure 7 Output channels for the input power against output coupler reflectivity for the maximum pump power of 43.8W.

Figure 8 Output power against output coupler reflectivity for various values of upconversion rate coefficient k (in m^3s^{-1}).

Figure 9 One-dimensional-cooling model structure

Figure 10 Temperature distribution near the waveguide core

Figure 11 Output power against output coupler reflectivity for various core temperatures.

Figure 12 Output power against output coupler reflectivity for four 60W diode pump lasers.

Figure 1

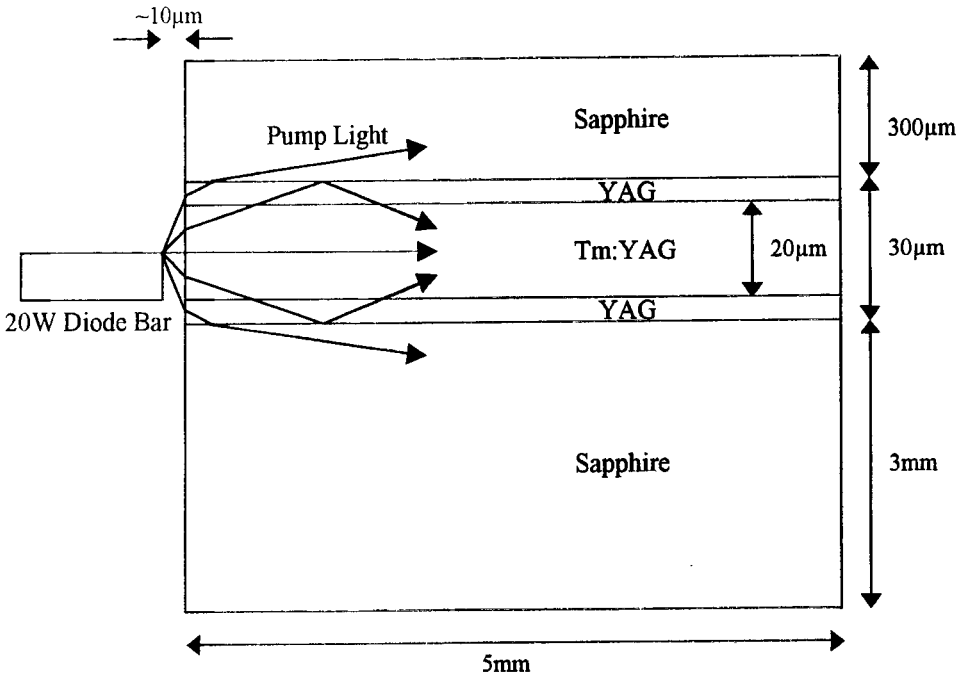
~10μm
Pump Light
Sapphire
300μm
YAG
Tm:YAG
20μm
30μm
YAG
20W Diode Bar
Sapphire
3mm
5mm

Figure 2

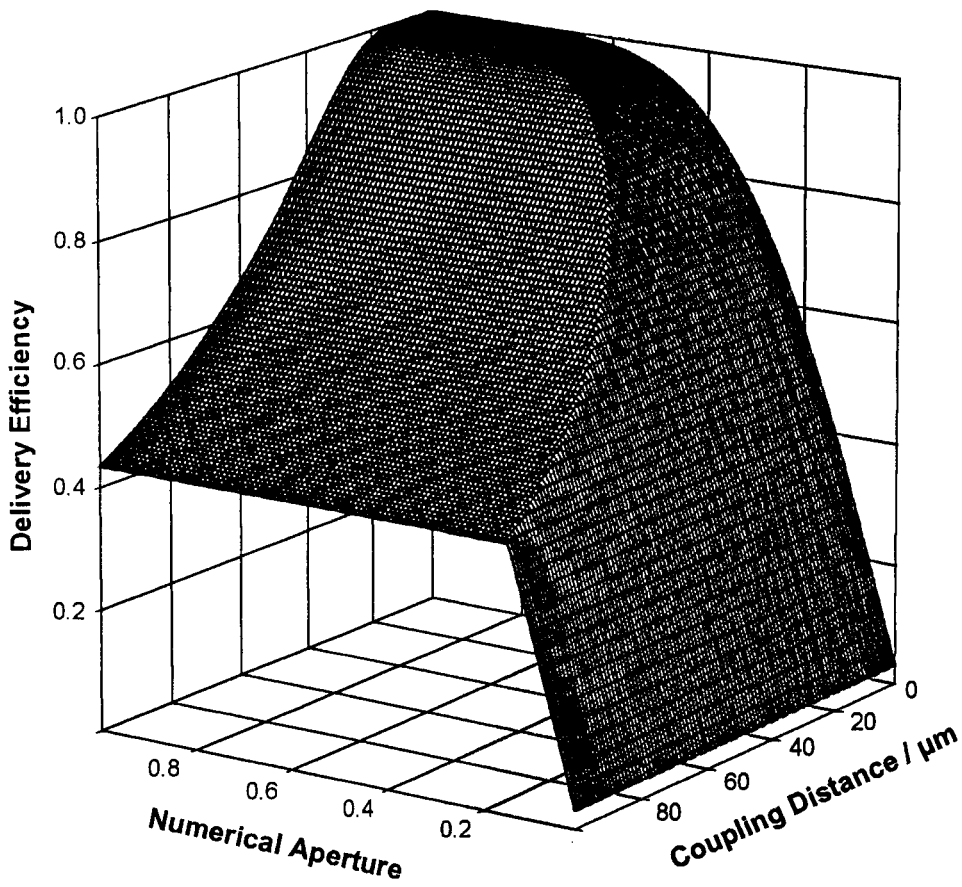
Delivery Efficiency
1.0
0.8
0.6
0.4
0.2
0.8
0.6
0.4
0.2
Numerical Aperture
0
20
40
60
80
Coupling Distance / µm

Figure 3

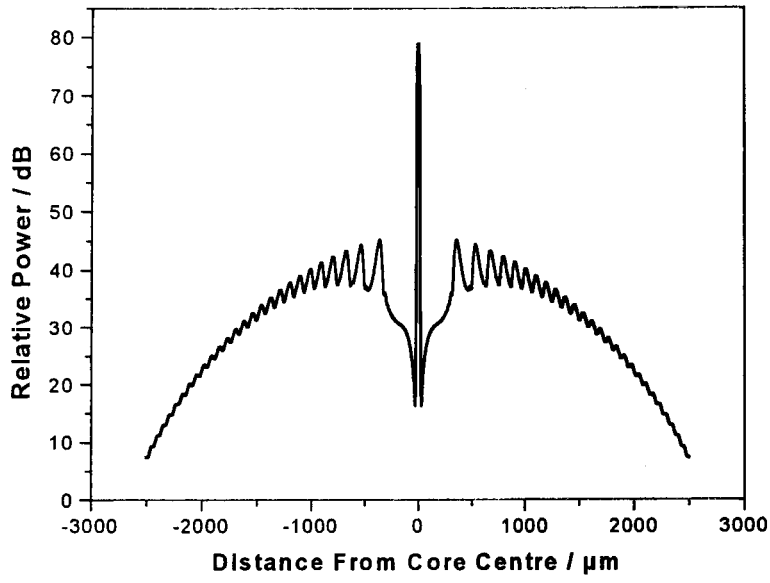
Relative Power / dB
80
70
60
50
40
30
20
10
0
-3000
-2000
-1000
0
1000
2000
3000
Distance From Core Centre / µm

Figure 4

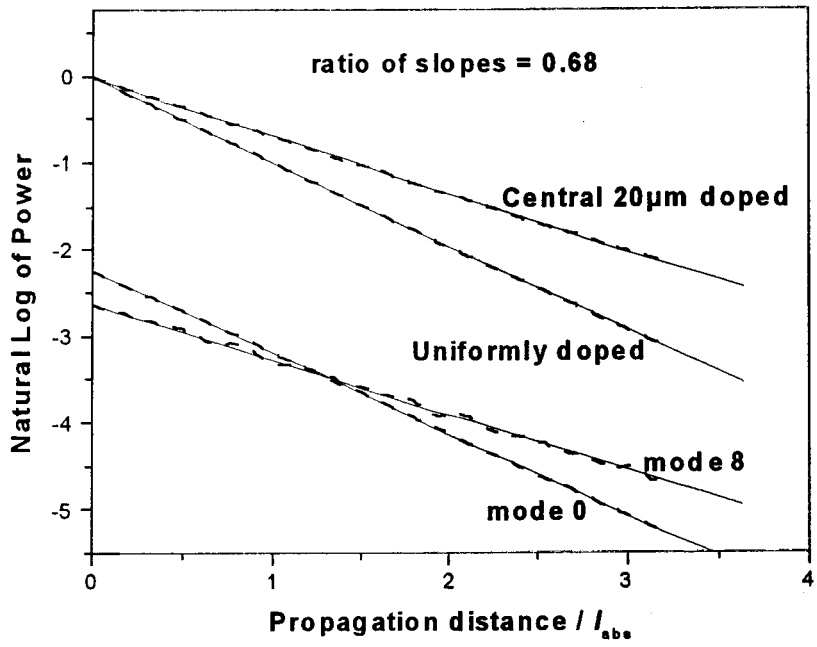
ratio of slopes = 0.68
Central 20μm doped
Uniformly doped
mode 8
mode 0
Natural Log of Power
0
-1
-2
-3
-4
-5
0
1
2
3
4
Propagation distance / l_{abs}

Figure 5

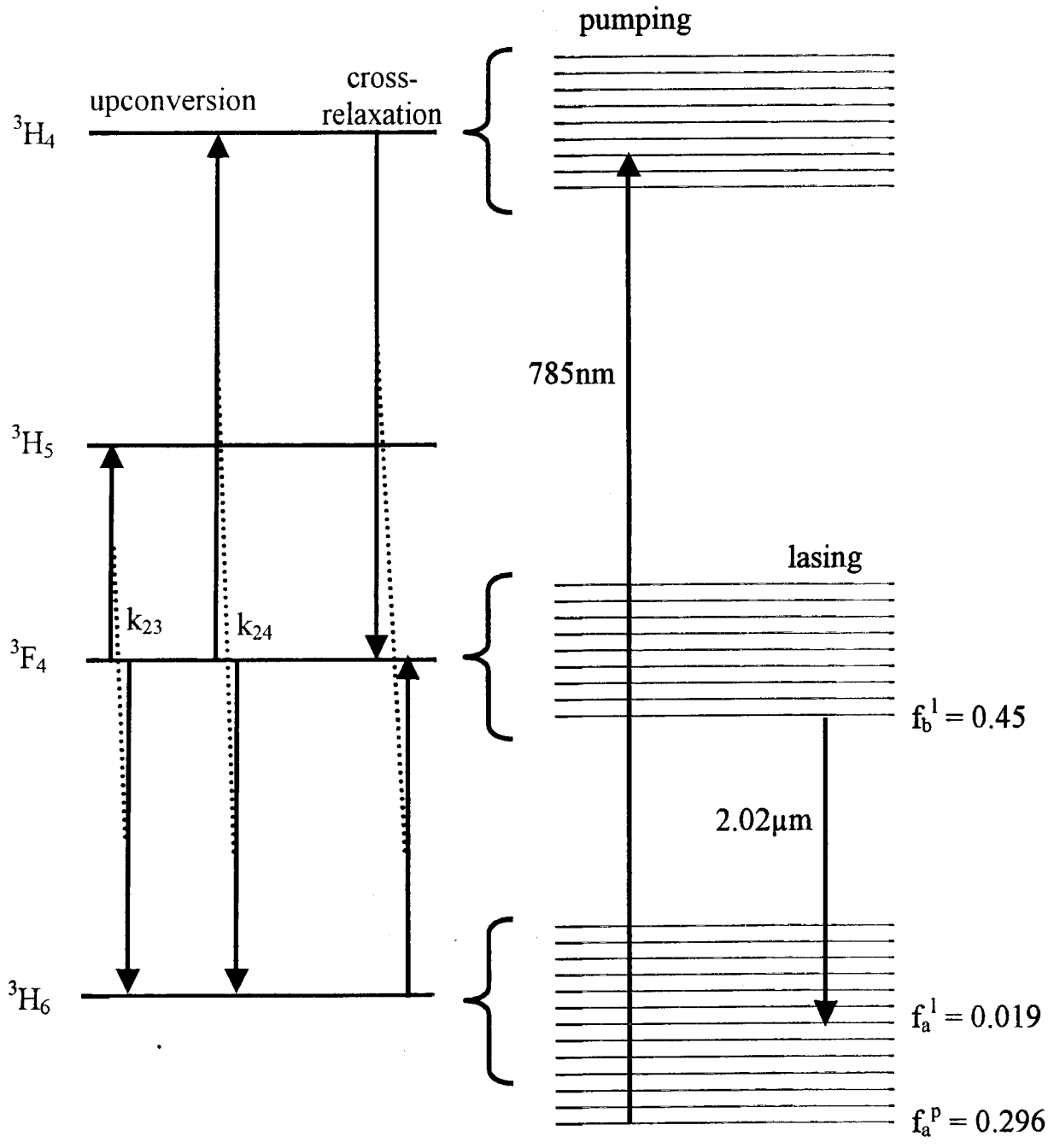

Tm^{3+}:YAG

Figure 6

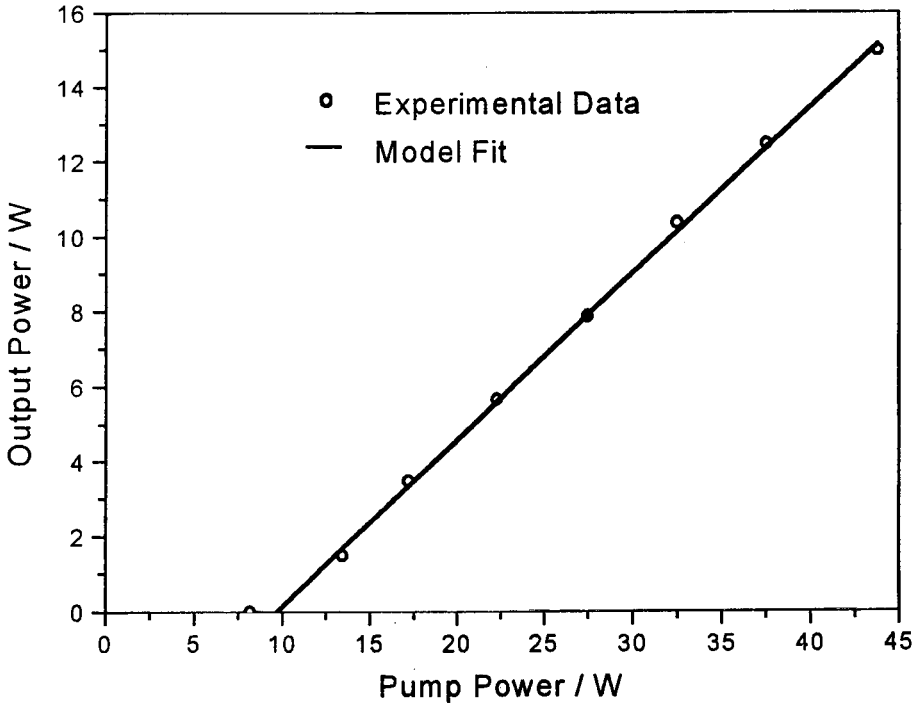
Experimental Data
Model Fit
Output Power / W
Pump Power / W
0
2
4
6
8
10
12
14
16
0
5
10
15
20
25
30
35
40
45

Figure 7

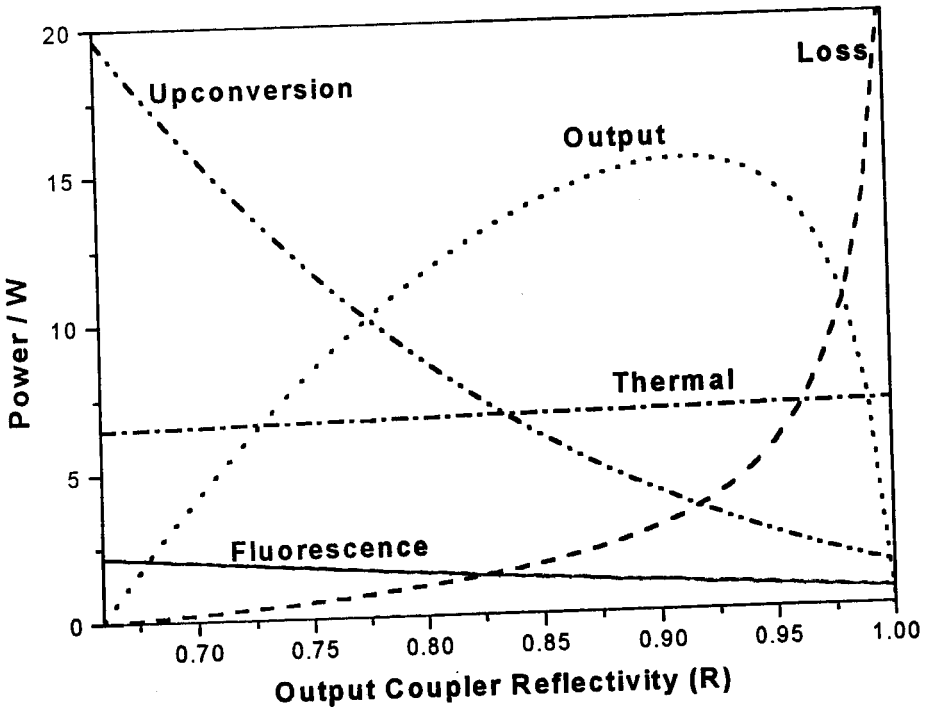
Loss
Upconversion
Output
Thermal
Fluorescence
Power / W
20
15
10
5
0
0.70
0.75
0.80
0.85
0.90
0.95
1.00
Output Coupler Reflectivity (R)

Figure 8

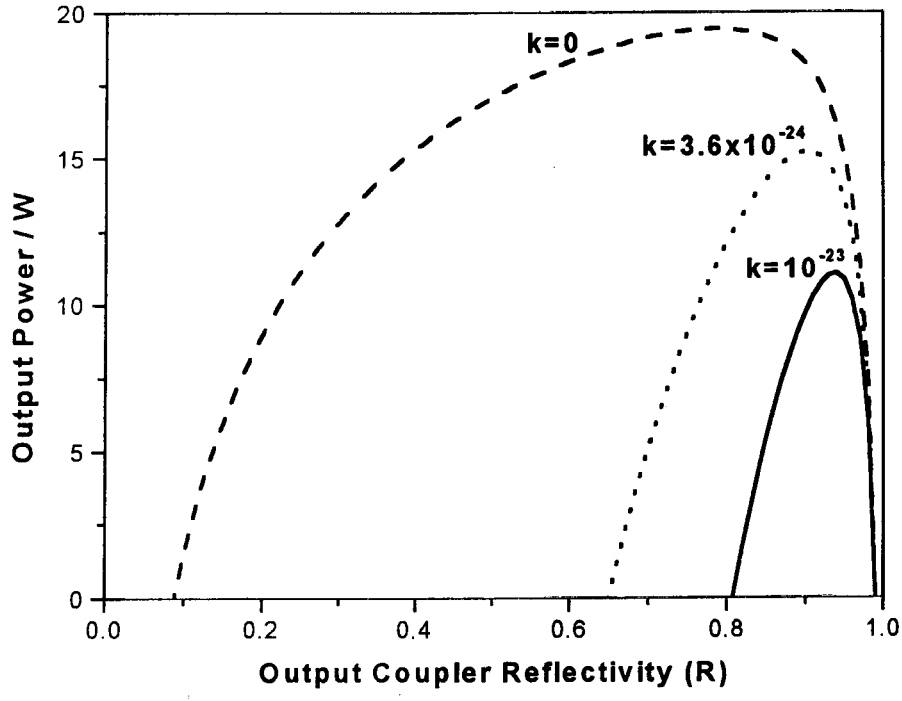
k=0
k=3.6x10^-24
k=10^-23
Output Power / W
Output Coupler Reflectivity (R)
0
5
10
15
20
0.0
0.2
0.4
0.6
0.8
1.0

Figure 9

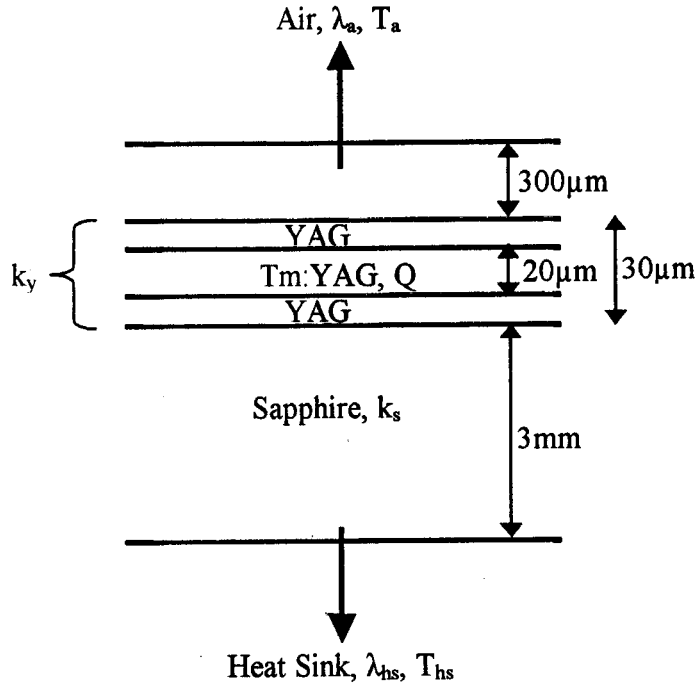
Air, λ_a, T_a
300µm
YAG
k_y
Tm:YAG, Q
20µm
30µm
YAG
Sapphire, k_s
3mm
Heat Sink, λ_{hs}, T_{hs}

Figure 10

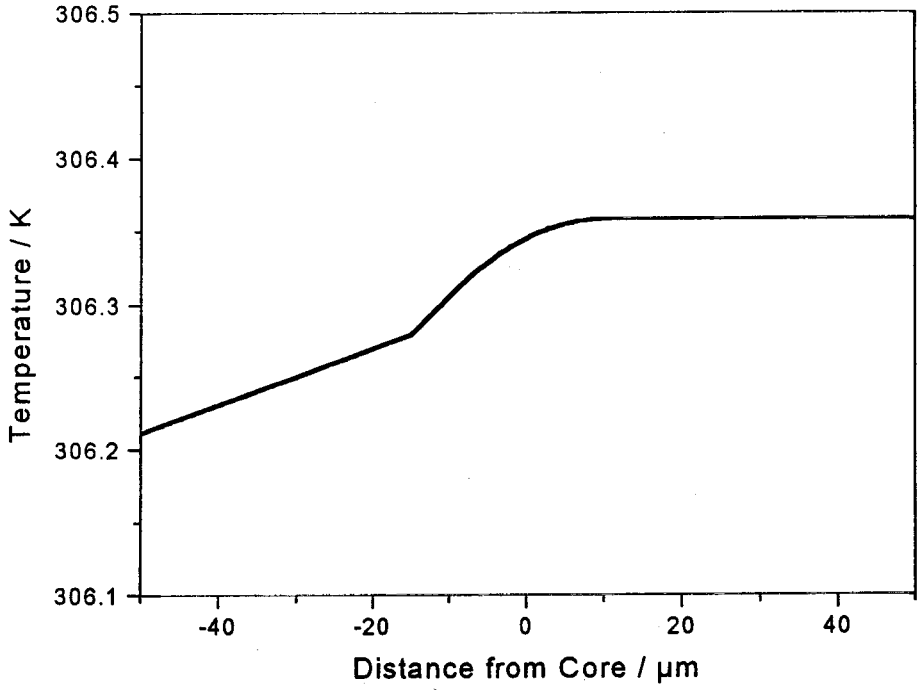
306.5
306.4
306.3
306.2
306.1
Temperature / K
-40
-20
0
20
40
Distance from Core / µm

Figure 11

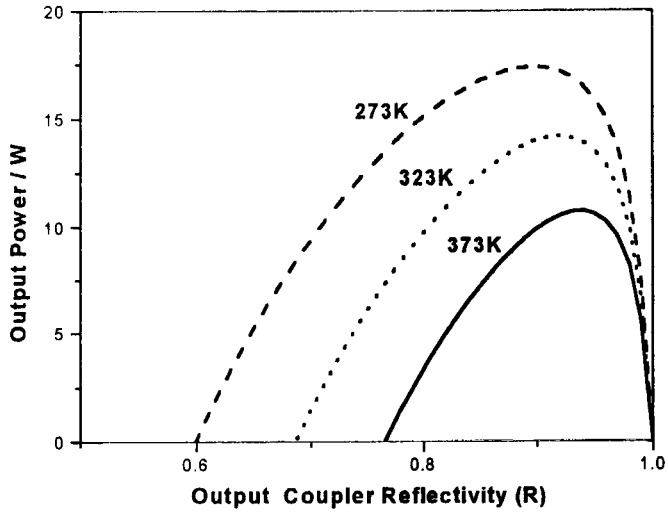
20
15
10
5
0
Output Power / W
273K
323K
373K
0.6
0.8
1.0
Output Coupler Reflectivity (R)

Figure 12

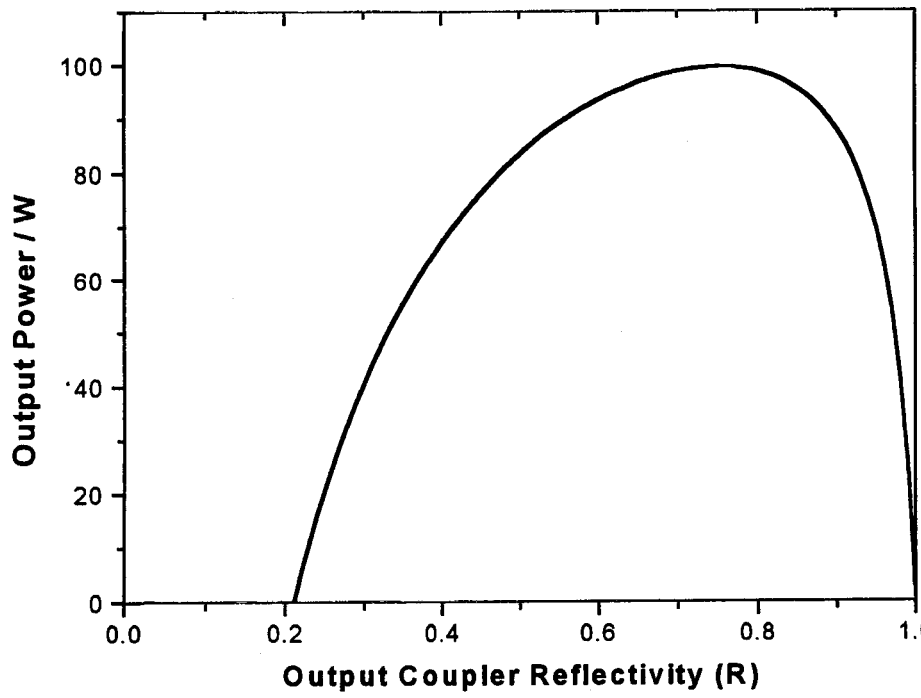
Output Power / W
100
80
60
40
20
0
0.0
0.2
0.4
0.6
0.8
1.0
Output Coupler Reflectivity (R)

References

[1] E.C.Honea, R.J.Beach, S.B.Sutton, J.A.Speth, S.C.Mitchell, J.A.Skidmore, M.A.Emanuel, and S.A.Payne, "115W Tm:YAG diode-pumped solid-state laser", *IEEE J. Quantum Electron.*, vol. QE-33, pp. 1592-1600, 1997.

[2] K.S.Lai, P.B.Phua, R.F.Wu, Y.L.Lim, Ernest Lau, S.W.Toh, B.T.Toh, and A.Chng, "120-W continuous-wave diode-pumped Tm:YAG laser", *Opt. Lett.*, vol. 25, pp.1591-1593, 2000.

[3] A.Rameix, C.Borel, B.Chambaz, B.Ferrand, D.P.Shepherd, T.J.Warburton, D.C.Hanna, and A.C.Tropper, "An efficient, diode-pumped, 2μm Tm:YAG waveguide laser", *Opt. Commun.*, vol. 142, pp. 239-243, 1997.

[4} R.A.Hayward, W.A.Clarkson, P.W.Turner, J.Nilsson, A.B.Grudinin, and D.C.Hanna, "Efficient cladding-pumped Tm-doped silica fibre laser with high power singlemode output at 2μm", *Electr. Lett.*, vol. 36, pp. 711-712, 2000.

[5] J.I.Mackenzie, S.C.Mitchell, R.J.Beach, H.E.Meissner, and D.P.Shepherd, "A 15W diode-side-pumped Tm:YAG waveguide laser at 2μm", *Electr. Lett.*, vol. 37, pp. 898-899, 2001.

[6] R.J.Beach, "CW Theory of quasi-three level end-pumped oscillators", *Opt. Commun.*, vol. 123, pp. 385-393, 1996.

[7] J.B.Gruber, M.E.Hills, R.M.Macfarlane, C.A.Morrison, G.A.Turner, G.J.Quarles, G.J.Kintz, and L.Estorowitz, "Spectra and energy levels of Tm^{3+}:$Y_3Al_5O_{12}$", *Phys. Rev. B*, vol. 40, pp. 9464-9476, 1989.

[8] G.Rustad and K.Stenersen, "Modelling of laser-pumped Tm and Ho lasers accounting for upconversion and ground-state depletion", *IEEE J. Quantum Electron.*, vol. QE-32, pp. 1645-1655, 1996.

[9] L.B.Shaw, R.S.F.Chang, and N.Djeu, "Measurement of up-conversion energy-transfer probabilities in Ho:$Y_3Al_5O_{12}$ and Tm:$Y_3Al_5O_{12}$", *Phys. Rev. B*, vol. 50, pp. 6609-6619, 1994.

[10] C.L.Bonner, T.Bhutta, D.P.Shepherd, and A.C.Tropper, "Double-clad structures and proximity coupling for diode-bar-pumped planar waveguide lasers", *IEEE J. Quantum Electron.*, vol. QE-36, pp. 236-242, 2000.

[11] J.I.Mackenzie, C.Li, D.P.Shepherd, H.E.Meissner, and S.C.Mitchell, "Longitudinally diode-pumped Nd:YAG double-clad planar waveguide laser", *Opt. Lett.*, vol. 26, pp. 698-700, 2001.

[12] T.Nishimura and T.Omi, "Relation between laser characteristics and Nd ion concentration in Nd:YAG", *Jpn. J. Appl. Phys.*, vol. 14, pp. 1011-1016, 1975.

[13] Y.F.Chen, Y.P.Lan, and S.C.Wang, "Influence of energy-transfer upconversion on the performance of high-power diode-end-pumped cw lasers", *IEEE J. Quantum Electron.*, vol. QE-36, pp. 615-619, 2000.

[14] J.M.Eggleston, T.J.Kane, K.Kuhn, J.Unternahrer, and R.L.Byer, "The slab geometry – part I: theory", *IEEE J. Quantum Electron.*, vol. QE-20, pp. 289-301, 1984.

[15] D.P.Shepherd, S.J.Hettrick, C.Li, J.I.Mackenzie, R.J.Beach, S.C.Mitchell, and H.E.Meissner, "High-power planar dielectric waveguide lasers", *J. Phys. D*, to be published, vol. 34, 2001.

[16] R.J.Beach, S.C.Mitchell, H.E.Meissner, O.R.Meissner, W.F.Krupke, J.M.McMahon, W.J.Bennett, and D.P.Shepherd, "Continuous-wave and passively Q-switched cladding-pumped planar waveguide lasers", *Opt. Lett.*, vol. 26, pp.881-883, 2001.